

Research Article

Open Access



A stretchable all-nanofiber iontronic pressure sensor

Yigen Wu¹, Shuai Dong¹, Xiaojuan Li², Liguo Wen², Hongwei Shen², Mengjiao Li², Xin Liu¹, Yang Zhang¹, Guolong Zeng¹, Jianyi Zheng^{1,*}, Dezhi Wu^{1,*}

¹Pen-Tung Sah Institute of Micro-Nano Science and Technology, Xiamen University, Xiamen 361005, China.

²Beijing Smart-chip Microelectronics Technology Co., Ltd, Beijing 102211, China.

*Correspondence to: Prof. Jianyi Zheng, Prof. Dezhi Wu, Pen-Tung Sah Institute of Micro-Nano Science and Technology, No. 422, Siming South Road, Xiamen University, Xiamen 361005, China. E-mail: zjy@xmu.edu.cn; wdz@xmu.edu.cn

How to cite this article: Wu Y, Dong S, Li X, Wen L, Shen H, Li M, Liu X, Zhang Y, Zeng G, Zheng J, Wu D. A stretchable all-nanofiber iontronic pressure sensor. *Soft Sci* 2023;3:33. <https://dx.doi.org/10.20517/ss.2023.24>

Received: 19 May 2023 First Decision: 3 Jul 2023 Revised: 17 Jul 2023 Accepted: 28 Jul 2023 Published: 8 Oct 2023

Academic Editor: Chuanfei Guo Copy Editor: Dong-Li Li Production Editor: Dong-Li Li

Abstract

Flexible pressure sensors with high stretchability, sensitivity, and stability are undoubtedly urgently required for potential applications in intelligent soft robots, human-machine interaction, health monitoring, and other fields. However, most current flexible pressure sensors are unable to endure large deformation and are prone to performance degradation or even failure during frequent operation due to their multilayered structures. Here, we propose a stretchable all-nanofiber iontronic pressure sensor that is composed of ionic nanofiber membranes used as dielectric layers and liquid metal used as electrodes. This sensor exhibits a high sensitivity of 1.08 kPa^{-1} over a wide range of 0–300 kPa, with a fast response-relaxation time of about 18/22 ms and excellent stability. The high sensitivity comes from the electric double layer formed at the ionic film/electrode interface, while high stretchability and stability are enabled by in-situ encapsulated all-nanofiber structures. As a proof of concept, a prototype sensor array is integrated into a soft pneumatic gripper, demonstrating its capability of pressure perception and object recognition during the grasping process. Thus, the scheme provides another excellent strategy to fabricate stretchable pressure sensors with superb performance in terms of high stretchability, sensitivity, and stability.

Keywords: Electrospinning, all-nanofiber structures, stretchable iontronic pressure sensor, soft pneumatic gripper



© The Author(s) 2023. Open Access This article is licensed under a Creative Commons Attribution 4.0 International License (<https://creativecommons.org/licenses/by/4.0/>), which permits unrestricted use, sharing, adaptation, distribution and reproduction in any medium or format, for any purpose, even commercially, as long as you give appropriate credit to the original author(s) and the source, provide a link to the Creative Commons license, and indicate if changes were made.



www.softscijournal.com

INTRODUCTION

Haptic sensing capabilities that mimic the functionality of human fingers are highly desired for soft robots to improve their intelligence, especially for soft grippers. Flexible sensors, which transduce external stimuli into electronic signals, have been widely used in various applications, such as human-machine interaction^[1,2], wearable health monitoring^[3-5], and electronic skins (e-skin)^[6-8]. Integrating flexible pressure sensors into soft grippers can endow them with tactile perception for interacting with humans or the external environment more safely and stably. Stretchability is an important property of flexible sensors when applied to the curved and soft surfaces of soft robots. It ensures a stable sensing function even under dynamical mechanical deformations^[9,10]. In addition, high sensitivity is fundamental for guaranteeing that intelligent soft robots can detect subtle external stimuli in dynamic environments and achieve accurate feedback. Furthermore, flexible sensors should operate stably for extended periods in a harsh and complicated environment^[11]. Accordingly, flexible sensors with high sensitivity, stretchability, and stability are of great significance to achieve reliable sensory feedback for soft robots.

Over the last two decades, significant efforts have been dedicated to developing various types of flexible sensors, such as flexible piezo-resistive^[12,13], piezo-capacitive^[14-16], piezo-electric^[17,18], and triboelectric sensors^[19,20]. Among these, piezo-capacitive flexible pressure sensors have attracted great attention due to their advantages of low power consumption, low signal drift, and simple structures. A piezo-capacitive sensor consists of a trilayered structure comprising two parallel electrode layers and an inner dielectric layer. The capacitance change of traditional piezo-capacitive pressure sensors comes from structural deformation under external mechanical stimuli, leading to geometrical changes. The performance of piezo-capacitive pressure sensors can be improved by incorporating microstructures on the surface of electrodes or the dielectric layer. Previous studies have indicated that introducing microcones^[21,22], micropyramid arrays^[17,23], and micropillar arrays^[18,24,25], and more can effectively improve sensitivity, response speed, limit of detection (LOD), and other parameters. However, although microstructures can enhance compressibility and elasticity of the dielectric layer, the improvement of sensitivity for traditional capacitive pressure sensors is still limited due to the structural stiffening of microstructures^[26]. As the pressure increases, this can lead to finite changes of geometrical properties, further constraining sensitivity improvement. Defects of piezo-capacitive pressure sensors, including low sensitivity and low capacitance values typically only on the pF scale^[27], make the capacitance values susceptible to external disturbances.

Recently, the sensitivity of piezo-capacitive pressure sensors has been improved by using iontronic films as dielectric layers to construct iontronic pressure sensors. These iontronic films contain cations and anions, forming an interfacial electric double layer (EDL) when in contact with the electrode. The capacitance of the interfacial EDL is determined by the contact area between the iontronic layer and the electrode layer, and it is typically more than 1,000 times higher than that of traditional sensors^[28-30]. Compared with traditional piezo-capacitive sensors, iontronic pressure sensors exhibit extremely high initial capacitance and pressure sensitivity. However, existing iontronic pressure sensors face challenges due to their convoluted fabrication process, which involves constructing microstructures through costly or complex manufacturing approaches (e.g., photolithographic routes^[31,32], laser sculptures^[33,34], templated methods^[35,36], and others). Additionally, these sensors require layer-by-layer (LbL) assembly of each functional layer^[37-41]. Another primary issue associated with iontronic pressure sensors is their brittle stability because of the non-bonded interfaces^[42-44] and mechanical mismatch^[45,46] between each stacked functional layer (e.g., the electrode layer and inner dielectric layer). As a result, separation^[47-49] or delamination^[50,51] occurs under complex or large mechanical deformations, making them less desirable for practical applications. It is, thus, imperative, albeit challenging, to develop stretchable pressure sensors with high sensitivity and stability through a more straightforward approach.

In this article, we bring forward a stretchable all-nanofiber iontronic pressure sensor (SNIPS) with high sensitivity and stability, achieved using the manufacturing approach of electrospinning and stencil printing. The high sensitivity is realized through the interfacial EDL sensing mechanism and the microstructure of electrospun nanofibers. The SNIPS also provides a low detection limit of 50 Pa and a fast response speed. The stretchability of the sensor allows for integration on the surface of a pneumatic soft gripper with great conformability. Additionally, we successfully realized object recognition based on machine learning with an accuracy of 94%. Based on this facile method, the SNIPS offers an effective fabrication approach for e-skins of soft robots.

EXPERIMENTAL

Materials

The GO powder (purity > 99%, Sifma-Aldrich) has diameters ranging from 0.5 to 5 μm and thickness ranging from 0.8 to 1.2 nm. The PVDF-HFP pellets ($M_w = 3.0 \times 10^4$) and TPU pellets ($M_w = 6.0 \times 10^4$) were purchased from Aladdin Industric Inc. The ratio of Galinstan liquid metal (Shenyang Naijijie Scientific Instrument Co., Ltd., Shenyang, China.) was 68.5% Ga, 21.5% In, and 10% Sn. The iontronic liquid [EMIM][TFSI] with purity > 99% was purchased from Aladdin Industric Inc. The N,N-Dimethylacetamide (DMAC) was purchased from Sinopharm Chemical Reagent Co., Ltd, $M_w = 87.12$ g/mol.

Preparation of PVDF-HFP and PVDF-HFP/[EMIM][TFSI] nanofiber membrane

For a pristine PVDF-HFP nanofiber membrane, the PVDF-HFP pellets were dissolved in DMAC (concentration of 10 wt.%) and stirred (Huafeng, Jiangsu) at 60 °C for 8 h to prepare the PVDF-HFP precursor solution. The electrospinning parameters of PVDF-HFP nanofibers were an applied voltage of 10 kV, a collecting distance of 10 cm, and an ink propulsion speed of 300 $\mu\text{L}/\text{h}$ using a needle inner diameter of 210 μm . The iontronic PVDF-HFP/[EMIM][TFSI] precursor solution was prepared by mixing the iontronic liquid of [EMIM][TFSI] (mass ratios were 1:2, 1:1, and 2:1) in PVDF-HFP precursor solution, followed by stirring for 2 h. The PVDF-HFP/[EMIM][TFSI] nanofibers were then deposited onto a ground rotating roller (50 rpm). The electrospinning parameters were adjusted depending on the mass ratio of [EMIM][TFSI].

Fabrication of the all-nanofiber iontronic pressure sensor

The TPU pellets were dissolved in DMAC at 60 °C for preparing the TPU solution with 20 wt.%. Electrospinning was adopted to obtain TPU nanofibers at spinning parameters of voltage 12 kV, receiving distance of 15 cm, propulsion speed of 300 $\mu\text{l}/\text{h}$, and needle inner diameter of 210 μm . The GO powder was dissolved in DMAC under sonication (KQ2200DE, China) for 3 h with a concentration of 5% for preparing GO/TPU composites precursor solution. After that, the TPU pellets were added and electromagnetic mixing at room temperature for 6 h. The GO/TPU composite nanofiber membrane was achieved under electrospinning parameters: applied voltage of 10 kV, collecting distance of 160 mm and flow rate of 300 $\mu\text{L}/\text{h}$.

The SNIPS was constructed in four steps. Firstly, deposition of pristine TPU nanofibers was carried out under the processed parameters mentioned above for 2 h. Then, the GO/TPU composite nanofiber membrane was deposited through electrospinning GO/TPU precursor solution for 1 h. Subsequently, the bottom liquid metal electrode was patterned directly on the surface of the GO/TPU composite nanofiber membrane through screen printing, and fine copper wires were embedded to connect to measurement equipment. After the inner dielectric layer was put on the bottom liquid metal electrode, a thin adhesive layer of GO/TPU nanofibers was deposited through electrospinning GO/TPU precursor solution for 20 min, and the top liquid metal electrode was directly printed. Following this, the GO/TPU precursor solution was electrosprayed for 1 h. Lastly, the electrospun TPU solution was deposited for 2 h to cover the device.

Fabrication of the pneumatic soft gripper integrated with all-nanofiber iontronic pressure sensors

The pneumatic soft gripper was fabricated through a mold-casting method by pouring Dragon Skin 30 (Smooth-On, USA) into 3D-printed molds. Three molds (A, B, and C) were 3D printed (Lite 300HD, UnionTech Ltd., Shanghai, China) with light-sensitive resin (DSM Somo Imagine® 8000). Molds A and B were assembled together to construct the top layer, while mold C was used to construct the bottom layer. Liquid Dragon skin 30 (weight ratio of parts A and B was 1:1) was poured into corresponding molds and heated for 3 h under 80 °C; the top and bottom layers were bonded together by painting a thin layer of silicone rubber adhesive (Sil-Poxy, Smooth-On, USA) on the bonding interface after being released. Lastly, the liquid Dragon skin 30 was painted on the surface of the pneumatic soft finger, and a prepared iontronic pressure sensor array was covered. The integration of the sensor was completed after natural curing for 8 h. The three-finger pneumatic soft gripper is designed as a pneumatic network consisting of an extensible layer with discrete bellow-type chambers and an inextensible layer with a flat sheet structure. The soft finger produces a bending motion as the chambers inflate. The FEA method: FEA was performed by commercial software. The TPU nanofiber membrane used as the base of the sensor was modeled as a linear elastic material. The material parameters were Young's modulus of $E \sim 1.0$ MPa, Poisson's ratio of 0.4, and mass density of 1.23 g/cm³ according to experimental results. The iontronic nanofiber membrane was also modeled as a linear elastic material with Young's modulus of $E \sim 8.0$ MPa, Poisson's ratio of 0.35, and mass density of 1.8 g/cm³. A dielectric layer was randomly perforated with holes to simulate the high porosity of the iontronic nanofiber membrane. Contact interactions were set between the surfaces of the dielectric layer and the base. All contact interactions were assumed to be frictionless without penetration. The boundary condition of displacement set at the right side of the base was 25, and the left side was -25, both in the direction of U1. The length of the sensor was 100 and would be stretched to 150 (50%) during the simulation. Keyframes were chosen to evaluate the influence of the stretching on the stress distribution of the dielectric layer.

Characterization and measurements

The scanning electron microscope (SEM) images were captured by a field emission scanning electron microscope (SU-70, Hitachi, Japan). The static contact angle of liquid metal was measured through a Contact Angle Analyzer (JC2000D5H, Powereach, China). The resistance and capacitance were measured by a digital multimeter (Agilent 34401A, USA) and a precision LCR meter (Agilent E4980AL, Keysight, 1 kHz frequency, 500 mV applied voltage), respectively. Environmental temperature and relative humidity were measured by a measuring instrument (GM620, Shanghai Tianzhi Intelligent Technology Co. Ltd., China). Photographs and videos were captured with a Huawei smartphone (Mate 40 Pro, China).

RESULTS AND DISCUSSION

Fabrication process of the SNIPS

Figure 1A depicts that SNIPS consists of four functional layers. These layers include two pure thermoplastic polyurethane (TPU) nanofiber membranes, which are used as the top and bottom encapsulation layers. Additionally, two graphene oxide (GO)/TPU nanofiber membranes are used for printing liquid metal electrodes. The top and bottom printed liquid metal serves as electrodes for charge induction, while an electrospun iontronic nanofiber membrane acts as the inner dielectric layer. The precursor solution of the inner iontronic dielectric nanofiber membrane is prepared by mixing the iontronic liquid 1-ethyl-3-methylimidazolium bis(trifluoromethylsulfonyl)imide ([EMIM][TFSI]) into the high dielectric constant matrix of poly(vinylidene fluoride-co-hexafluoropropylene) (PVDF-HFP). The liquid metal electrodes and PVDF-HFP/[EMIM][TFSI] iontronic nanofiber membrane act as the pressure-sensitive unit for generating the EDL effect. Traditionally, the fabrication of piezo-capacitive pressure sensors typically

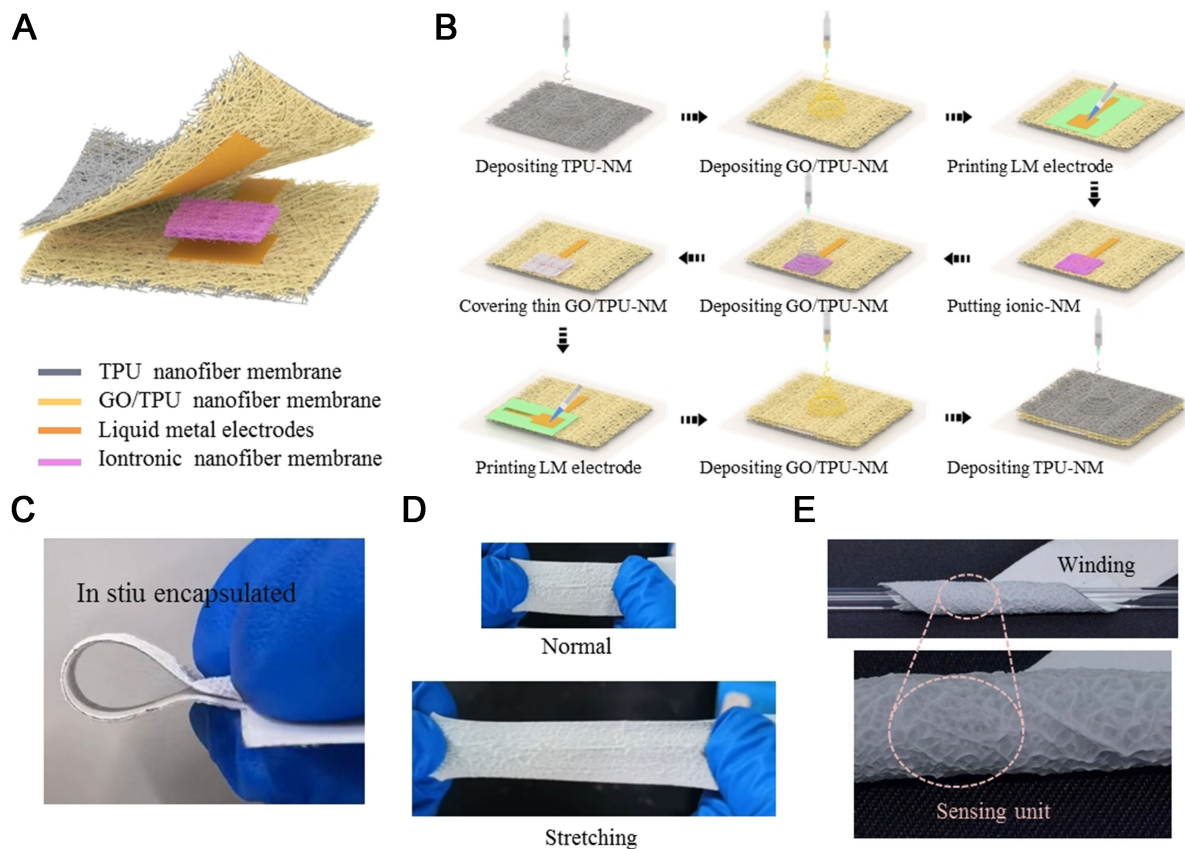


Figure 1. The structure and fabrication of the SNIPS. (A) Schematic diagram of the SNIPS structure; (B) Schematic illustration of the fabrication process using electrospinning and screen-printing approach; Photographs of the fabricated SNIPS enduring deformations of (C) bending, (D) stretching, and (E) wrapping. GO: Graphene oxide; SNIPS: stretchable all-nanofiber iontronic pressure sensor; TPU: thermoplastic polyurethane.

involves three steps: constructing the inner dielectric layer, creating the top and bottom electrodes, and encapsulating the device by assembling each layer. In contrast, our flexible pressure sensor is fabricated in a one-step facile electrohydrodynamic jet printing manufacturing approach. The schematic fabricating procedure is illustrated in Figure 1B. Electrospinning is adopted for depositing nanofibers to construct each functional layer, and liquid metal electrodes are patterned through stencil printing. The detailed fabrication process of the device and the inner iontronic PVDF-HFP/[EMIM][TFSI] nanofiber membrane is described in the “EXPERIMENTAL SECTION”.

The electrospun TPU nanofiber membrane is chosen as the substrate and encapsulation layer due to its high stretchability. Highly conductive liquid metal is patterned on the surface of the electrospun GO/TPU nanofiber membrane, which is constructed by incorporating GO with TPU. The GO/TPU is used as a bonding layer because the -OH groups provided by GO can in-situ form hydrogen bonds with the liquid metal oxide layer [Supplementary Figure 1]. These formed hydrogen bonds can improve the adhesion and wetting characteristics of liquid metal to the GO/TPU nanofiber membrane^[52]. As shown in Supplementary Figure 1A, the interfacial interaction between liquid metal and pristine TPU nanofibers is weak. However, as illustrated in Supplementary Figure 1B, liquid metal forms an interfacial interaction induced by hydrogen bonds with GO/TPU nanofibers. As shown in Supplementary Figure 2A, the morphology of electrospun TPU nanofiber is explicit, and the corresponding contact angle to liquid metal is 155°. After incorporating

GO with TPU, cross-link networks of GO/TPU nanofibers, induced by GO, are formed, and a corresponding contact angle of the liquid metal to GO/TPU nanofiber membrane is decreased to 127° [[Supplementary Figure 2B](#)]. Furthermore, [Supplementary Figure 3](#) illustrates that the maximum elongation of the TPU nanofiber membrane is 650%, with Young's modulus of about 0.5 MPa. For the GO/TPU nanofiber membrane, the maximum elongation is 480%, with Young's modulus of about 0.9 MPa, proving excellent flexibility and stretchability of both the GO nanofiber membrane and GO/TPU nanofiber membrane.

As mentioned above, typical capacitive pressure sensors are fabricated in multi-steps, requiring encapsulation, while our flexible pressure sensor is fabricated in a one-step procedure. The electrospun nanofibers interconnect and stack together during the depositing process. As shown in [Figure 1C](#), the multilayered device exhibits distinct structural integrity, benefitting from this fascinating process. This ensures excellent stability and durability. [Figure 1D](#) demonstrates that the SNIPS exhibits high strength and toughness, allowing it to withstand stretching deformation. Moreover, the mechanical compliance of the device enables it to wrap around a cylindrical surface [[Figure 1E](#)]. Additionally, the PVDF-HFP/[EMIM][TFSI] dielectric layer is encased in TPU nanofiber packing materials to keep oxygen and water away from the inner iontronic nanofiber membrane, ensuring long-term stability.

Pressure sensing mechanism and key components design of the SNIPS

The SNIPS exhibits extremely high sensitivity by utilizing the EDL-sensitive mechanism that the supercapacitance generates at the interface between the electrolytic and electronic components. This is achieved by sandwiching the iontronic PVDF-HFP/[EMIM][TFSI] nanofiber membrane, containing massive positive and negative charged ion pairs, between the top and bottom liquid metal electrodes. The pressure sensing mechanism is illustrated in [Figure 2A](#) and [B](#). Electrons on the liquid metal electrodes and the ions in the dielectric nanofibers attract and accumulate in a nanometer distance, which leads to an ultrahigh capacitance value that is essentially proportional to the electronic-ionic contact area between the electrode and the inner dielectric layer. As illustrated in [Figure 2A](#), under the unloading situation, only a few iontronic nanofibers contact the electrode, resulting in a low initial capacitance. As illustrated in [Figure 2B](#), after pressure is applied, the electronic-ionic contact area increases as the iontronic nanofiber membrane is compressed. More iontronic nanofibers begin to touch the electrodes and result in the increase of EDL area and, accordingly, an increase of capacitance. The compression of nanofiber membranes leads to two changes: the change of thickness and the contact area of EDL capacitors, both of which result in the change of capacitance. According to the equivalent model of EDL, the capacitance of SNIPS comes from the direct plane-parallel capacitor and the top and bottom EDL capacitors (C_{EDL1} and C_{EDL2}). Since the EDL capacitance is far higher than that of the plane-parallel capacitor, the capacitance of SNIPS is mainly determined by the EDL capacitance.

The electrospun pure PVDF-HFP nanofibers exhibit relatively smooth surfaces and are uniformly interleaved and deposited together [[Supplementary Figure 4](#)]. However, the electrospun iontronic PVDF-HFP/[EMIM][TFSI] nanofiber membrane, formed by mixing iontronic liquid of [EMIM][TFSI] into PVDF-HFP, contains massive positive and negative charged ion pairs distributed within the PVDF-HFP nanofibers. The interface between [EMIM][TFSI] and PVDF-HFP matrix involves noncovalent interactions, which leads to a well-stated bonding of ions to PVDF-HFP nanofibers. As illustrated in [Supplementary Figure 5](#), a higher content of [EMIM][TFSI] results in more iontronic solids precipitated on the surface of PVDF-HFP nanofibers and finer fiber diameter. The conductivity of the precursor PVDF-HFP/[EMIM][TFSI] solution increases with the addition of [EMIM][TFSI], and the jet is prone to furcate and whip during the spinning process. Eventually, the electrospun nanofibers entangle together

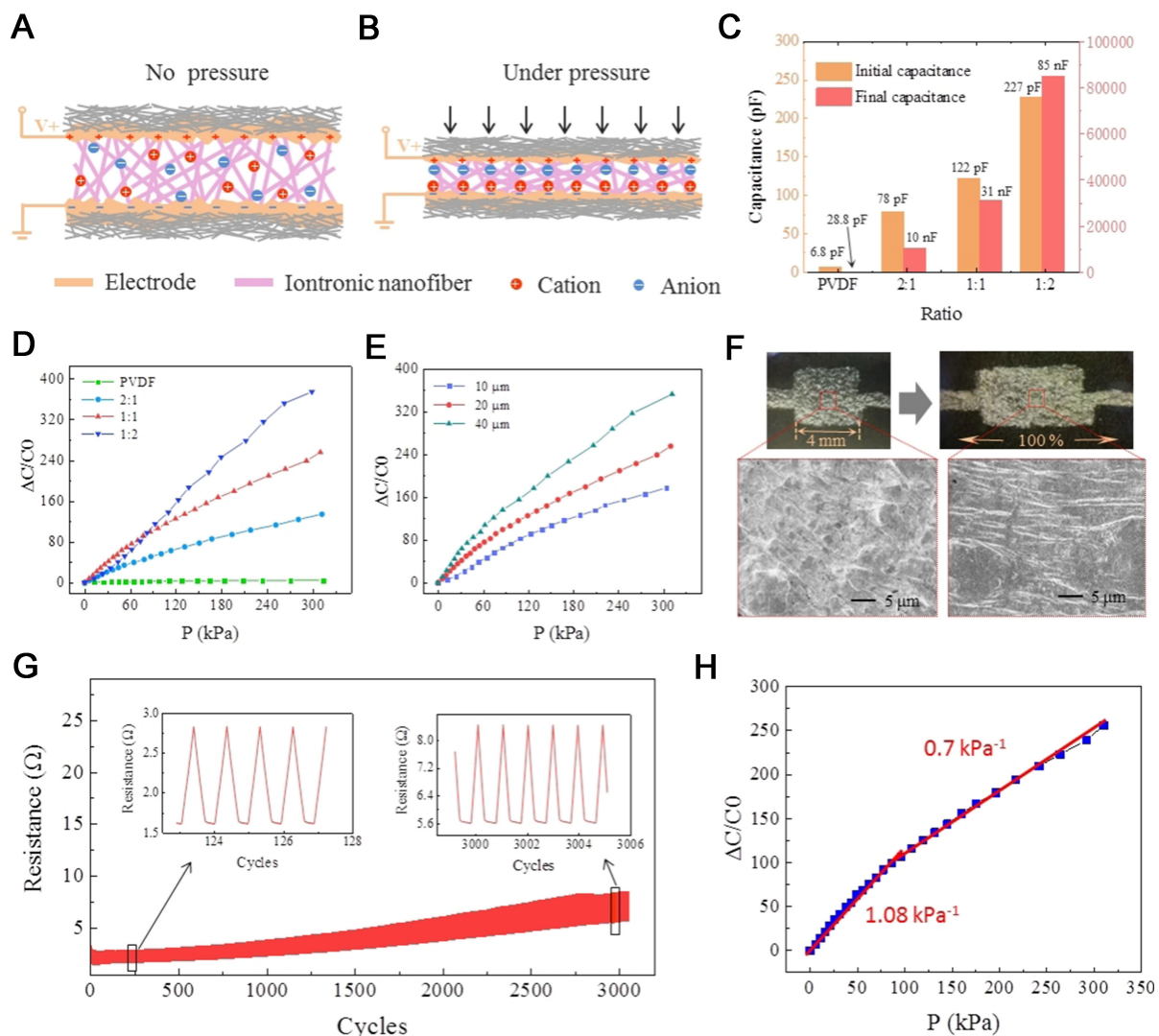


Figure 2. The sensing mechanism of the SNIPS. Schematic illustration of the SNIPS structure (A) before and (B) after applying pressure; (C) The initial capacitance and final capacitance of sensors packed different dielectric layers; (D) Normalized change in capacitance as a function of the pressure of SNIPS packed different dielectric layers; (E) Normalized capacitive change as a function of the pressure of SNIPS with different dielectric layers; (F) Photographs and SEM images of the liquid metal electrode surface at the initial and stretching states; (G) Normalized resist change of the liquid metal electrode stretched to a strain of 100% over 3,000 cycles; (H) The relative capacitance variation of the SNIPS under different pressures. SNIPS: stretchable all-nanofiber iontronic pressure sensor; SEM: scanning electron microscope.

[Supplementary Figure 6] when the content of [EMIM][TFSI] to PVDF-HFP ratio exceeds 2:1, resulting in a very uneven electrospun iontronic PVDF-HFP/[EMIM][TFSI] nanofiber membrane, and the morphology of nanofibers is poor [Supplementary Figure 7].

In order to assess the effect of [EMIM][TFSI] contents on the capacitance value and pressure sensing performance, different inner dielectric layers, including PVDF-HFP nanofiber membranes and PVDF-HFP/[EMIM][TFSI] nanofiber membranes with different [EMIM][TFSI] contents (1:2, 1:1, and 2:1), are prepared. Figure 2C shows the initial capacitance without applied pressure and the final capacitance after applying 300 kPa pressure of devices packed with prepared dielectric layers. The initial capacitance C_0 is about 6.8 pF, and the final capacitance C is about 28.8 pF for the sensor packed with PVDF-HFP nanofiber

membranes, which only exhibits a slight increase in capacitance variation. After adding [EMIM][TFSI], both the initial capacitance and final capacitance increase, and the capacitance value increases with the increase of [EMIM][TFSI] contents. For [EMIM][TFSI] contents of 1:1, the initial capacitance C_0 is about 78 pF, and the final capacitance C is about 10 nF. Sensors using PVDF-HFP/[EMIM][TFSI] nanofiber membranes with contents of 2:1 exhibit maximum initial capacitance. It proved that the capacitance of EDL is typically more than 1,000 times higher than that of traditional sensors, and the capacitance greatly changed under applied pressure for sensors using PVDF-HFP/[EMIM][TFSI] nanofiber membranes as dielectric layers.

To further explore the effect of [EMIM][TFSI] contents on the pressure sensing performance, the capacitance of different sensors under different applied pressures is measured. As shown in [Figure 2D](#), the capacitive response of all the sensors increases with applied pressure ranging from 0 to 300 kPa. Sensors using PVDF-HFP nanofiber membranes as dielectric layers exhibit the worst response performance, and sensors using PVDF-HFP/[EMIM][TFSI] nanofiber membranes with contents of 2:1 as dielectric layers exhibit the highest response performance. As shown in [Supplementary Figure 8](#), for sensors using PVDF-HFP nanofiber membranes as dielectric layers, the capacitance only increases three times and four times after applying pressures of 100 kPa and 300 kPa, respectively, and exhibits poor linearity in the whole pressure range. The sensor using PVDF-HFP/[EMIM][TFSI] nanofiber membranes with contents of 2:1 exhibits the highest response performance because more [EMIM][TFSI] contents result in a higher capacitance density. However, the conductivity of the precursor ink for electrospinning ionotronic nanofiber membrane increases with the addition of [EMIM][TFSI]. The spinnability becomes poor for precursor ink with higher conductivity, and the electrospun nanofibers cannot form a continuous porous network and are easy to agglomerate together and form larger clusters [[Supplementary Figure 7](#)]. As shown in [Figure 2D](#), sensors using PVDF-HFP/[EMIM][TFSI] nanofiber membranes with [EMIM][TFSI] contents of 2:1 exhibit unstable sensing performance, and the linearity is poor. For comparison, sensors with [EMIM][TFSI] contents of 1:1 performance have high sensitivity and good linearity in the whole pressure range. The pressure sensing performance is also influenced by the thickness of the iontronic nanofiber membrane. As shown in [Figure 2E](#), larger thickness leads to higher sensing performance as larger thickness results in better compressibility, and the change of EDL area becomes larger under external pressure. However, larger thickness leads to larger sizes of the SNIPS, which limits the application scenarios.

Flexible electrodes are essential components for flexible sensors. Conventional electrodes of capacitive sensors face challenges in striking a balance between conductivity and stretchability, which can influence the stability of the device. In this work, we patterned liquid metal on the surface of the GO/TPU nanofiber membrane through stencil printing. Incorporating GO with TPU can enhance the interfacial bonding between liquid metal and GO/TPU nanofiber membranes, leading to high stability of the patterned liquid metal structure during the stretching process. We print a liquid metal electrode with an area of $4 \times 4 \text{ mm}^2$ on the surface of the GO/TPU nanofiber membrane and observe the morphology during the stretching process. As shown in [Figure 2F](#), the liquid metal can uniformly coat the surface of the GO/TPU nanofiber membrane. After the electrode is stretched over 100%, the liquid metal, bonded by the substrate, remains smooth and flat and can deform in the stretching direction without structural breakage. After subjecting the electrode to 3,000 stretching cycles at 100% strain, the initial resistance of liquid metal changes from 1.5 to 5.6 Ω [[Figure 2G](#)]. Throughout the stretching process, the maximum resistance of the electrode remains below 10 Ω (the resistance increases from 5.6 to 8.2 Ω for the 3,000th stretching cycle). The observation of little drift in resistance and no failure of the structure of the liquid metal electrode enables the device to achieve excellent stability under high stretching deformation.

Lastly, we constructed a device using a packed PVDF-HFP/[EMIM][TFSI] nanofiber membrane with thickness of 20 μm and an [EMIM][TFSI] content ratio of 1:1, with a sensing area of $4 \times 4 \text{ mm}^2$. Sensitivity is a key parameter of pressure sensors, defined as $S = \delta(\Delta C/C_0)/\delta P$, where C_0 is the initial capacitance, P is the applied pressure, and $\Delta C = (C - C_0)$ is the relative change of capacitance under the applied pressure P . **Figure 2H** shows that capacitance responses of the SNIPS, which have two stages. High sensitivity of 1.08 kPa^{-1} is observed in the pressure range of 0–100 kPa. The second stage, from 100 to 300 kPa, exhibits a linear sensing behavior with sensitivity of 0.8 kPa^{-1} . The all-fabric structure, porous iontronic dielectric nanofiber membranes, and electrical properties of liquid metal electrodes play critical roles in improving the sensing performance.

Sensing performance of the SNIPS

The sensing performances, including dynamic performance, LOD, response/relaxation time, and durability, were investigated. We first test the real-time capacitive responses of SNIPS under loading/unloading pressures of 5, 15, 60, and 100 kPa for five cycles at each applied pressure. As shown in the testing results demonstrated in **Figure 3A**, the pressure sensor not only presents stable capacitance responses with high repeatability but also is capable of responding to continuous pressure with different loading amplitudes. These results indicate that SNIPS can potentially detect dynamic consecutive pressure. As shown in **Figure 3B**, the sensor could accurately respond to an ultralow pressure of 50 Pa, with the capacitance increasing from 121 to 122.2 pF. To investigate the response time of SNIPS, a pressure of 50 kPa is carefully loaded onto the device and then quickly removed after 0.5 s. As depicted in **Figure 3C**, the capacitance of SNIPS rapidly ascended within 18 ms as the external pressure applied, and then it maintained at a stable value. As the pressure was removed, the capacitance promptly recovered to its initial value in about 22 ms (as shown in the insets of **Figure 3C**). To investigate the durability, the SNIPS is subject to 5,000 compression and release cycles at a repeated pressure of 100 kPa. **Figure 3D** exhibits that no fatigue or capacitance drift appears after cyclic compression, confirming the high durability of SNIPS. Additionally, the iontronic pressure sensor is in-situ sealed, ensuring that the structure of the sensor remains stable under different compressions.

Considering that most flexible sensors are inevitably affected by stretching, we proceed to characterize the sensing performances of our sensor in stretching conditions. We applied stretching up to 50% strain (each strain of 10%, 30%, 40%, and 50% is repeated five times) and measured the corresponding capacitance change. As shown in **Figure 4A**, the capacitance of SNIPS increases with the stretching. The capacitance response to a strain of 10% approximately changes from 121 to 170 pF. With an increase in stretching, more change of capacitance is produced. However, when the stretching exceeds the strain of 30%, the capacitance will change abruptly and become unstable. For a strain of 50%, the device exhibits a maximum deviation of approximately 85% (121 to 210 pF). **Figure 4B** and **Supplementary Video 1** demonstrate the results of finite element analysis (FEA) that simulates the stretching process of the sensor. More details of the FEA simulation can be found in the “EXPERIMENTAL SECTION”. For a low stretching rate, the TPU layer exhibits more obvious local stress, and nearly no local stress occurs for the iontronic layer. Upon the strain exceeding 30%, local stress appears and becomes concentrated in a specific region of the ionotronic layer with increasing stretching. The nonuniform distribution of stress on the ionotronic nanofiber membrane results in abrupt and unstable capacitance changes.

To confirm the stability under stretched conditions, we applied 30% strain on SNIPS for 3,000 cycles and measured the capacitive variation. As shown in **Figure 4C**, the capacitance stably changed from 121 to 165 pF with the stretching, and no change of initial capacitance was observed after cyclic stretching. The pressure-sensing response curves of sensors at different stretching conditions are shown in **Figure 4D**. Our

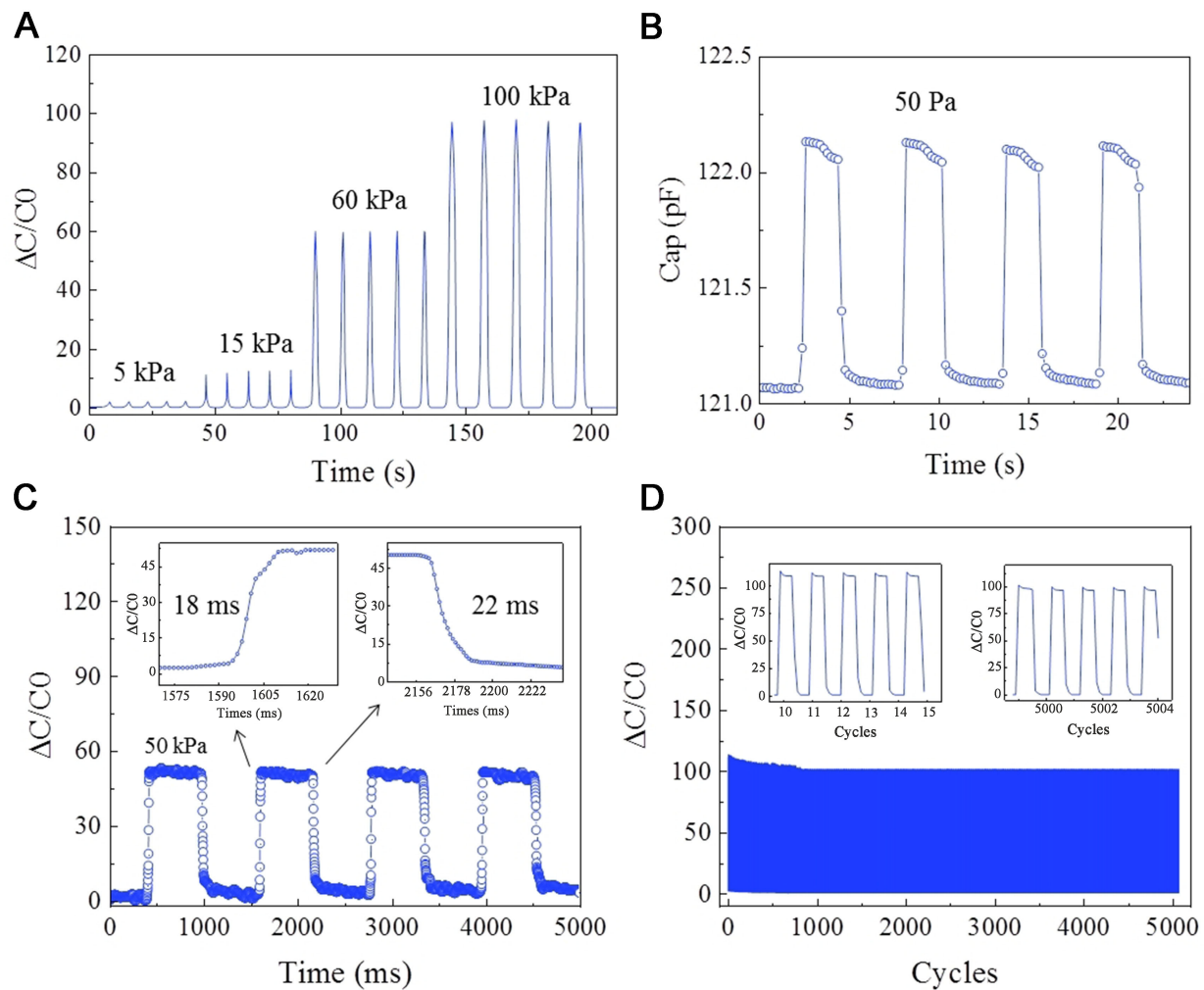


Figure 3. Sensing properties of the SNIPS with optimized configuration. (A) Dynamic response of relative capacitance variation loading with different pressures; (B) The LOD test of the SNIPS; (C) Transient response of relative capacitance variation to an applied pressure of 50 kPa. The insets show the response/relaxation time of SNIPS; (D) Long-term stability tested by compression and release over 5,000 cycles under external pressure of 250 kPa. LOD: Limit of detection; SNIPS: stretchable all-nanofiber iontronic pressure sensor.

sensor can properly operate under no-strain conditions and stretching deformation of 10% and 30% strains, which reflect the steadiness and accuracy of pressure sensing performance. We ascribe the high stability performance to the stacked structure of nanofibers, as well as the liquid metal electrode. The structure of liquid metal remains stable, benefitting from the selective adhesion of liquid metal to different layers. As shown in [Supplementary Figure 9](#), no structural damage is observed for liquid metal is adhesive to the GO/TPU nanofiber membrane and is repellent to the inner iontronic nanofiber membrane. The Young's modulus of the iontronic nanofiber membrane is about 1 MPa [[Supplementary Figure 10](#)], which is far larger than that of the TPU nanofiber membrane and the GO/TPU nanofiber membrane. The gradient distribution of Young's modulus not only reduces the stress concentration of the inner iontronic layer but also ensures the structural stability of the iontronic layer during the compressive process [[Supplementary Figure 11](#)].

To improve the stretchability of the all-nanofiber iontronic pressure sensor, PVA solution with high Young's modulus is coated around the iontronic nanofiber membrane, forming a rectangle structure to

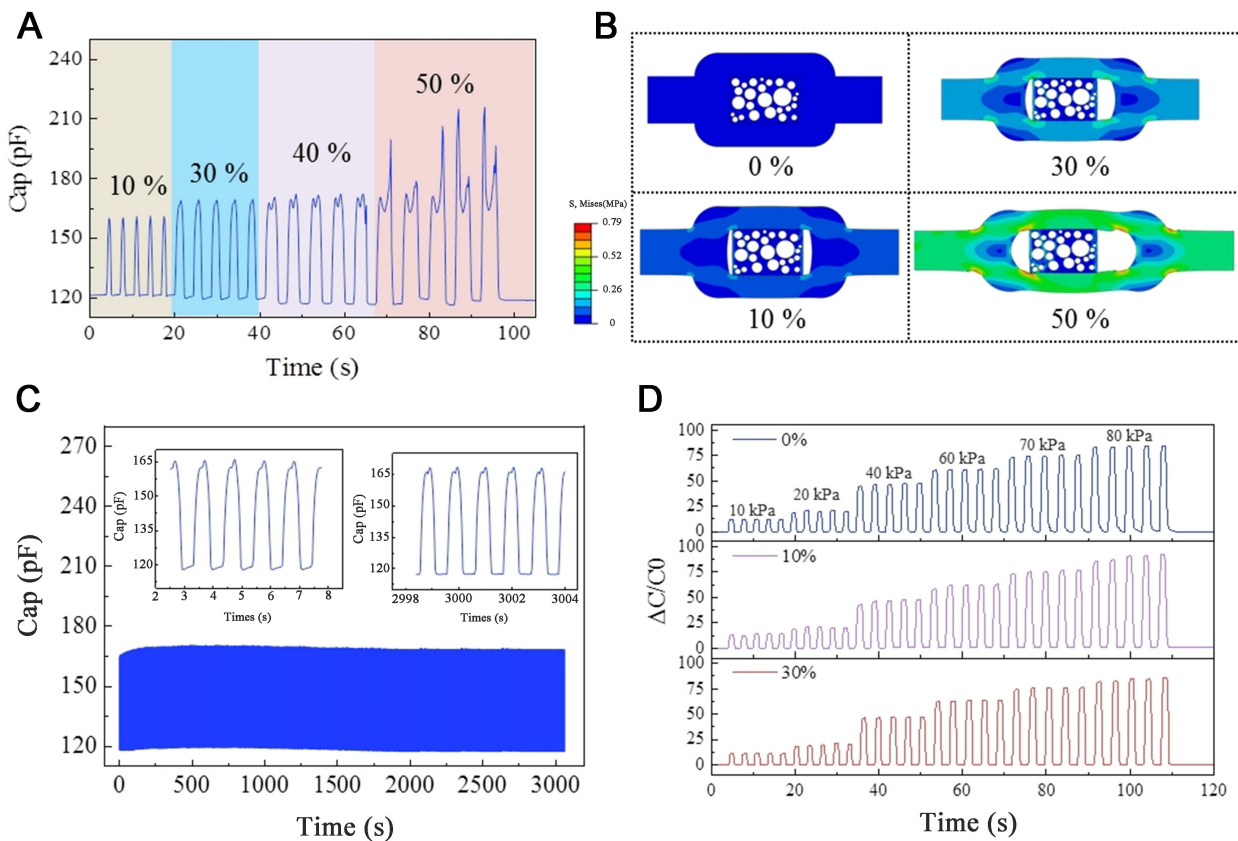


Figure 4. Performances of the stretchable SNIPS under a state of stretching deformation. (A) The variation of initial capacitance of SNIPS under stretching up to 50%; (B) Finite element modeling of stress distribution in a device under applied stretching up to 50%. The encapsulated layer and dielectric layer are modeled as incompressible materials with Young's moduli of 0.5 MPa and 60 MPa, respectively; (C) The capacitance changes during stretching-recovery cycles over 5,000 times under strains of 30%; (D) Normalized capacitance changes of the SNIPS under different strains and pressures. SNIPS: Stretchable all-nanofiber iontronic pressure sensor.

reduce the stress concentration during the compression process. As shown in [Supplementary Figure 12A](#), the constructed all-nanofiber iontronic pressure sensor with the PVA-coated dielectric layer maintains stable sensing performance with a 10 kPa gradient pressure under 50% stretching. As shown in [Supplementary Figure 12B](#), no loss of sensitivity is observed under stretching of 0%, 30%, 40%, and 50%, proving that the constructed all-nanofiber iontronic pressure sensor with the PVA-coated dielectric layer possesses high stability and stretchability.

We subject the constructed SNIPS with the PVA-coated dielectric layer to different external pressures of 100 kPa with diverse frequencies under a condition of 50% stretching. As shown in [Supplementary Figure 13](#), the PVA-coated SNIPS maintains a stable output response under 100 kPa external pressure with frequencies of 1, 1.5, 2.5, and 3 Hz, proving its dynamic sensing performance under stretching deformation. In conclusion, the constructed all-nanofiber iontronic pressure sensor with a PVA-coated dielectric layer can stretch up to 50% strain.

E-skins integration for pneumatic soft gripper

As illustrated in [Supplementary Table 1](#), our SNIPS offers a combination of high sensitivity, stability, and stretchability compared to other capacitive pressure sensors. The high stretchability and stability of SNIPS allow us to measure tactile sensing for soft robots. Herein, a sensor array, including three devices with a

response unit of $4 \times 4 \text{ mm}^2$, is attached to the surface of a homemade pneumatic soft gripper. Figure 5A demonstrates that the compliance mechanical properties allow the sensor to maintain intimate contact with the surface of soft robots even over a large deformation. We measured the capacitive response of the integrated sensor when the soft fingers were pneumatically bent without air pressure. The capacitance changes from 121 to 136 pF [Figure 5B] under an air pressure of 30 kPa. The capacitive variation stably remains at 15.4 pF [Figure 5C]. However, the capacitance changes from 121 to 490 pF [Figure 5D] when the soft finger grabs a bottle under an air pressure of 30 kPa. The capacitance stably remained at 220.3 pF [Figure 5E], indicating that the integrated pressure sensor is less affected by bending deformation. As shown in Figure 5F, the sensor enables quantitative recognition of different types of touched objects, including PDMS, bottles, and fabrics. There is a minimal change of capacitance resulting from touching PDMS for its softness. The capacitive variation is significant for stress concentration caused by microstructures of fabrics.

Real-time monitoring of grasping strength is of great significance for soft grippers. Based on the excellent pressure sensing performance of SNIPS, we used the integrated sensor to detect the falling of grasped objects [Figure 5G and Supplementary Video 2]. Jitter is a very common problem for manipulator robots and leads to accidental falling of grasped objects and even object damage. Apart from grasping force detection, the sensor can also detect jitter signals during the grasping process. As shown in Figure 5H, characteristic waveforms of jitter signals caused by hand movement can be observed. From the enlarged view of the inset, the peaks can reflect the strength of hand shaking [Supplementary Video 3]. These demonstrations prove that our sensor is useful in tactile sensing ability for soft robots.

Application of pressure distribution detection and target identification

The tough integration of the sensor-robot also enables the application of detecting pressure distribution. As shown in Figure 6A and B, we used sensory-integrated soft grippers to grasp an empty bottle container (weight: 15 g) and a bottle container full of water (weight: 235 g). As shown in Figure 6A, we first examined the capacitance changes during grasping an empty bottle. Because the weight of the empty bottle is lighter, the contact force focuses on the middle position, and the grasped pressure gradually varies according to corresponding pressure mapping. By contrast, when the weight of the grasped object increases, the pressure distribution focuses on the bottom position since the grasped object is relatively heavy [Figure 6B]. The intelligent soft gripper has a potential application in identifying grasped objects based on machine learning. We adopted the GDBT method for training, and Figure 6C is the diagram for identifying. Each object is grasped for 100 times [Supplementary Figure 14 and 15]. The result of the confusion matrix is shown in Figure 6D, showing that the pneumatic soft gripper integrated with SNIPS has recognition accuracies of > 94% for all the objects. We expect that our sensor can be used to achieve stable haptic sensations for soft robots.

CONCLUSIONS

In summary, we have constructed SNIPS for soft robots. Owing to the excellent mechanical properties of nanofibers, the excellent electrical performance of liquid metal electrodes, and EDL interfacial effects, the fabricated SNIPS shows high sensitivity of 1.08 kPa^{-1} , a fast response time superior to human skin, and excellent stability. The proposed pressure sensor can endow tactile sensing ability for soft robots. We demonstrate applications of detecting grasping force and jitter signals. Lastly, the intelligent soft gripper achieved grasped object identification with a recognition accuracy of > 94% based on machine learning.

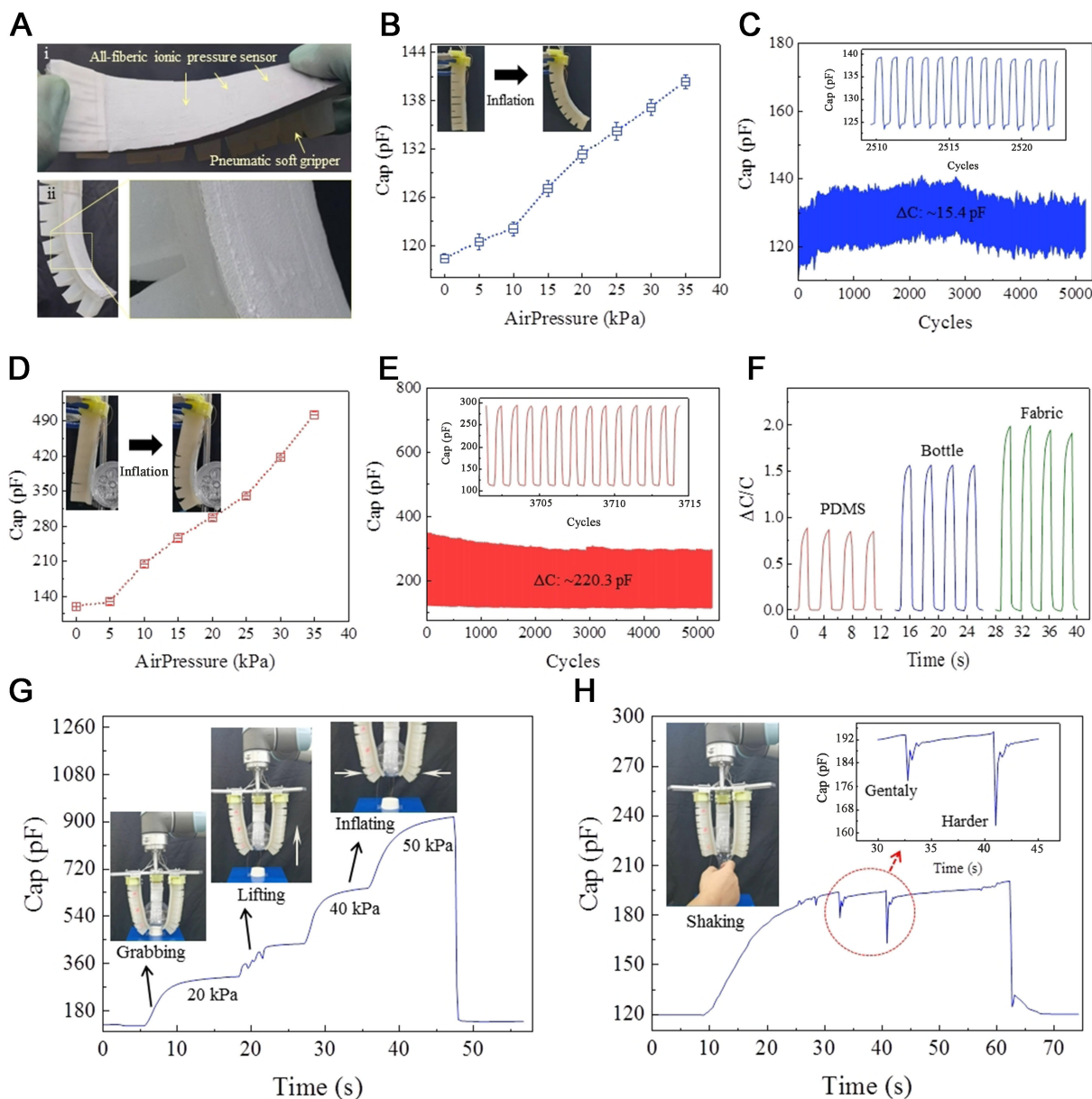


Figure 5. Soft robot-sensor integration and its applications in grasping objects. (A) Photographs of a pneumatic soft gripper merge with a sensor array consisting of three sensors; (B) The capacitance change for a sensor integrated on the surface of pneumatic soft fingers under different air pressures; the pneumatic soft finger does not touch objects during the bending process; (C) The corresponding capacitance change during inflating-deflating cycles over 5,000 times; (D) The capacitance change for a sensor integrated on the surface of pneumatic soft fingers under different air pressures; the pneumatic soft finger touches a hard bottle during the bending process; (E) The corresponding capacitance change during touching-releasing cycles over 5,000 times; (F) Capacitance change when touching different objects; (G) Tactile sensing by grasping a plastic ball (weight: 25 g); (H) Capacitance change when shaking the grasped object.

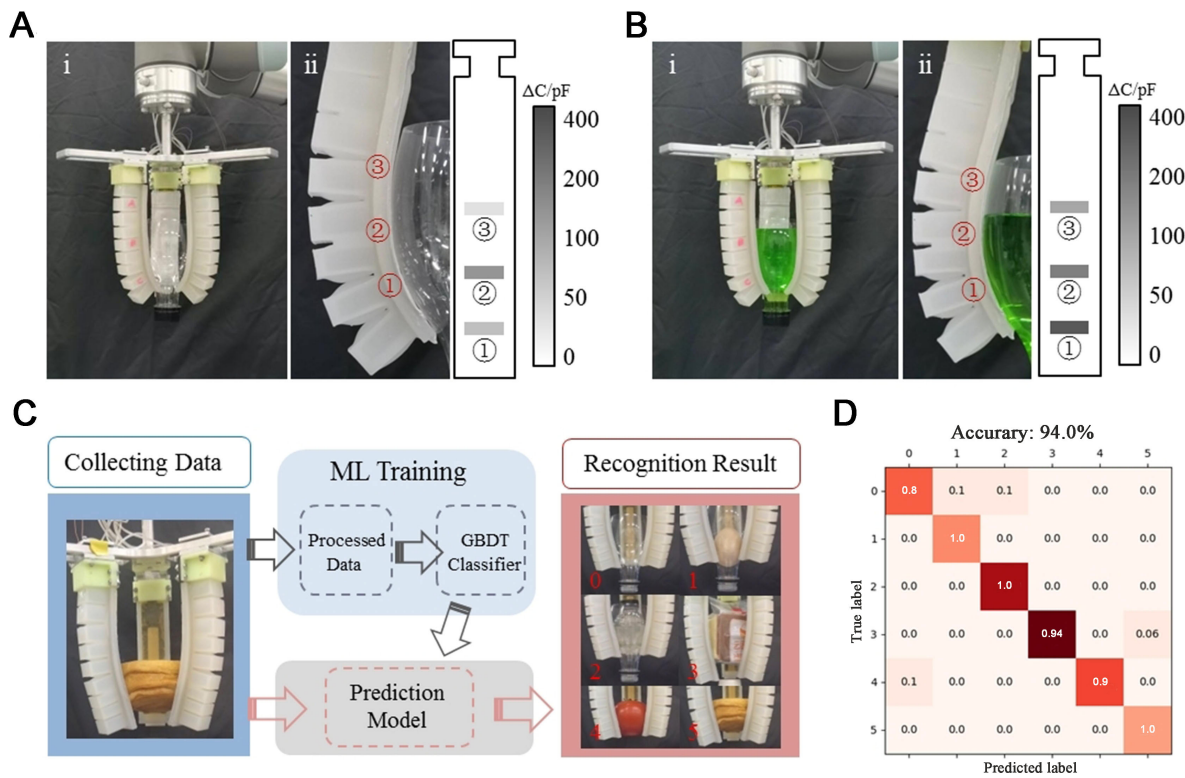


Figure 6. Use of the intelligent soft gripper-integrated stretchable pressure for detecting the gripping force position and target recognition. (A) Optical images of grasping an empty bottle and corresponding mapping of the capacitance changes; (B) Optical images of grasping a bottle full of water and corresponding mapping of the capacitance changes; (C) The illustration of the target recognition process, including sensor data collection, machine learning training, and real-time prediction; (D) Recognition confusion matrix of recognizing grasped targets.

DECLARATIONS

Authors' contributions

Conceptualization, methodology, investigation, writing-original draft, writing-review, and editing: Wu Y
 Investigation, writing, and editing: Dong S
 Methodology, writing, and editing: Li X
 Writing and editing: Wen L, Shen H
 Investigation: Li M
 Software, formal analysis, writing- review, and editing: Liu X, Zhang Y, Zeng G
 Methodology, supervision, and project administration: Zheng J
 Conceptualization, supervision, project administration, and resource funding acquisition: Wu D

Availability of data and materials

The data presented in this study are available upon request from the corresponding author.

Financial support and sponsorship

This work is in part supported by the National Natural Science Foundation of China (52075464), the Laboratory Open Fund of Beijing Smart-chip Microelectronics Technology Co., Ltd. (No. SGSC0000MNQT2207234), Natural Science Foundation of Xiamen (3502Z20227176), and the Program Granted by Special Funds from the Central Government to Guide Local Scientific and Technological Development (2021Syzup068).

Conflicts of interest

All authors declared that there are no conflicts of interest.

Ethical approval and consent to participate

Not applicable.

Consent for publication

Not applicable.

Copyright

© The Author(s) 2023.

REFERENCES

1. Zhou Z, Chen K, Li X, et al. Sign-to-speech translation using machine-learning-assisted stretchable sensor arrays. *Nat Electron* 2020;3:571-8. [DOI](#)
2. Yin R, Wang D, Zhao S, Lou Z, Shen G. Wearable sensors-enabled human-machine interaction systems: from design to application. *Adv Funct Mater* 2021;31:2008936. [DOI](#)
3. Sugiyama M, Uemura T, Kondo M, et al. An ultraflexible organic differential amplifier for recording electrocardiograms. *Nat Electron* 2019;2:351-60. [DOI](#)
4. Wang C, Hwang D, Yu Z, et al. User-interactive electronic skin for instantaneous pressure visualization. *Nat Mater* 2013;12:899-904. [DOI](#)
5. Patel S, Erheem F, Zhao M, et al. Wearable electronics for skin wound monitoring and healing. *Soft Sci* 2022;2:9. [DOI](#) [PubMed](#) [PMC](#)
6. Wehner M, Truby RL, Fitzgerald DJ, et al. An integrated design and fabrication strategy for entirely soft, autonomous robots. *Nature* 2016;536:451-5. [DOI](#)
7. Araromi OA, Graule MA, Dorsey KL, et al. Ultra-sensitive and resilient compliant strain gauges for soft machines. *Nature* 2020;587:219-24. [DOI](#)
8. Jin T, Sun Z, Li L, et al. Triboelectric nanogenerator sensors for soft robotics aiming at digital twin applications. *Nat Commun* 2020;11:5381. [DOI](#) [PubMed](#) [PMC](#)
9. Zhao H, Huang R, Shepherd RF. Curvature control of soft orthotics via low cost solid-state optics. In: 2016 IEEE International Conference on Robotics and Automation (ICRA); 2016 May 16-21; Stockholm, Sweden. IEEE; 2016. p. 4008-13. [DOI](#)
10. Wang H, Totaro M, Beccai L. Toward perceptive soft robots: progress and challenges. *Adv Sci* 2018;5:1800541. [DOI](#) [PubMed](#) [PMC](#)
11. Yamaguchi T, Kashiwagi T, Arie T, Akita S, Takei K. Human-like electronic skin-integrated soft robotic hand. *Adv Intell Syst* 2019;1:1900018. [DOI](#)
12. Zhang C, Zhou W, Geng D, et al. Laser direct writing and characterizations of flexible piezoresistive sensors with microstructures. *Opto-Electron Adv* 2021;4:200061. [DOI](#)
13. Qi K, He J, Wang H, et al. A highly stretchable nanofiber-based electronic skin with pressure-, strain-, and flexion-sensitive properties for health and motion monitoring. *ACS Appl Mater Interfaces* 2017;9:42951-60. [DOI](#)
14. Chen L, Lu M, Yang H, et al. Textile-based capacitive sensor for physical rehabilitation via surface topological modification. *ACS Nano* 2020;14:8191-201. [DOI](#) [PubMed](#)
15. Lee S, Franklin S, Hassani FA, et al. Nanomesh pressure sensor for monitoring finger manipulation without sensory interference. *Science* 2020;370:966-70. [DOI](#)
16. Ha KH, Zhang W, Jang H, et al. Highly sensitive capacitive pressure sensors over a wide pressure range enabled by the hybrid responses of a highly porous nanocomposite. *Adv Mater* 2021;33:2170382. [DOI](#)
17. Chang C, Tran VH, Wang J, Fuh YK, Lin L. Direct-write piezoelectric polymeric nanogenerator with high energy conversion efficiency. *Nano Lett* 2010;10:726-31. [DOI](#) [PubMed](#)
18. Deng W, Yang T, Jin L, et al. Cowpea-structured PVDF/ZnO nanofibers based flexible self-powered piezoelectric bending motion sensor towards remote control of gestures. *Nano Energy* 2019;55:516-25. [DOI](#)
19. Chen J, Chen B, Han K, Tang W, Wang ZL. A triboelectric nanogenerator as a self-powered sensor for a soft-rigid hybrid actuator. *Adv Mater Technol* 2019;4:1900337. [DOI](#)
20. Wen F, Sun Z, He T, et al. Machine learning glove using self-powered conductive superhydrophobic triboelectric textile for gesture recognition in VR/AR applications. *Adv Sci* 2020;7:2000261. [DOI](#) [PubMed](#) [PMC](#)
21. Zheng S, Zhang J, Deng H, Du Y, Shi X. Chitin derived nitrogen-doped porous carbons with ultrahigh specific surface area and tailored hierarchical porosity for high performance supercapacitors. *J Bioresour Bioprod* 2021;6:142-51. [DOI](#)
22. Mahanty B, Ghosh SK, Maity K, Roy K, Sarkar S, Mandal D. All-fiber pyro- and piezo-electric nanogenerator for IoT based self-powered health-care monitoring†. *Mater Adv* 2021;2:4370-9. [DOI](#)

23. Li X, Fan YJ, Li HY, et al. Ultracomfortable hierarchical nanonetwork for highly sensitive pressure sensor. *ACS Nano* 2020;14:9605-12. [DOI](#)
24. Pan L, Han L, Liu H, Zhao J, Dong Y, Wang X. Flexible sensor based on hair-like microstructured ionic hydrogel with high sensitivity for pulse wave detection. *J Chem Eng* 2022;450:137929. [DOI](#)
25. Veeramuthu L, Cho CJ, Venkatesan M, et al. Muscle fibers inspired electrospun nanostructures reinforced conductive fibers for smart wearable optoelectronics and energy generators. *Nano Energy* 2022;101:107592. [DOI](#)
26. Yuan Z, Shen G, Pan C, Wang ZL. Flexible sliding sensor for simultaneous monitoring deformation and displacement on a robotic hand/arm. *Nano Energy* 2020;73:104764. [DOI](#)
27. Shen Z, Zhu X, Majidi C, Gu G. Cutaneous ionogel mechanoreceptors for soft machines, physiological sensing, and amputee prostheses. *Adv Mater* 2021;33:2102069. [DOI](#) [PubMed](#)
28. Zhao C, Wang Y, Tang G, et al. Ionic flexible sensors: mechanisms, materials, structures, and applications. *Adv Funct Mater* 2022;32:2110417. [DOI](#)
29. Niu H, Li H, Gao S, et al. Perception-to-cognition tactile sensing based on artificial-intelligence-motivated human full-skin bionic electronic skin. *Adv Mater* 2022;34:2270225. [DOI](#)
30. Tian Z, Qin W, Wang Y, et al. Ultra-stable strain/ humidity dual-functional flexible wearable sensor based on brush-like AgNPs@CNTs@TPU heterogeneous structure. *Colloids Surf A Physicochem Eng Asp* 2023;670:131398. [DOI](#)
31. Mannsfeld SCB, Tee BCK, Stoltberg RM, et al. Highly sensitive flexible pressure sensors with microstructured rubber dielectric layers. *Nat Mater* 2010;9:859-64. [DOI](#)
32. Lu P, Wang L, Zhu P, et al. Iontronic pressure sensor with high sensitivity and linear response over a wide pressure range based on soft micropillared electrodes. *Sci Bull* 2021;66:1091-100. [DOI](#)
33. Wan ZF, Chen X, Gu M. Laser scribed graphene for supercapacitors. *Opto-Electron Adv* 2021;4:200079. [DOI](#)
34. Zhang L, Pan J, Zhang Z, et al. Ultrasensitive skin-like wearable optical sensors based on glass micro/nanofibers. *Opto-Electron Adv* 2020;3:190022. [DOI](#)
35. Qiu Z, Wan Y, Zhou W, et al. Ionic skin with biomimetic dielectric layer templated from *Calathea Zebrine* leaf. *Adv Funct Mater* 2018;28:1802343. [DOI](#)
36. Zhang P, Zhang J, Li Y, Huang L. Flexible and high sensitive capacitive pressure sensor with microstructured electrode inspired by ginkgo leaf. *J Phys D Appl Phys* 2021;54:465401. [DOI](#)
37. Lin Q, Huang J, Yang J, et al. Highly sensitive flexible iontronic pressure sensor for fingertip pulse monitoring. *Adv Healthc Mater* 2020;9:2001023. [DOI](#)
38. Li Z, Zhu M, Shen J, Qiu Q, Yu J, Ding B. All-fiber structured electronic skin with high elasticity and breathability. *Adv Funct Mater* 2020;30:1908411. [DOI](#)
39. Lin X, Xue H, Li F, Mei H, Zhao H, Zhang T. All-nanofibrous ionic capacitive pressure sensor for wearable applications. *ACS Appl Mater Interfaces* 2022;14:31385-95. [DOI](#)
40. Cui X, Chen J, Wu W, et al. Flexible and breathable all-nanofiber iontronic pressure sensors with ultraviolet shielding and antibacterial performances for wearable electronics. *Nano Energy* 2022;95:107022. [DOI](#)
41. Guo Y, Yin F, Li Y, Shen G, Lee JC. Incorporating wireless strategies to wearable devices enabled by a photocurable hydrogel for monitoring pressure information (Adv. Mater. 29/2023). *Adv Mater* 2023;35:2370208. [DOI](#)
42. Tao K, Chen Z, Yu J, et al. Ultra-sensitive, deformable, and transparent triboelectric tactile sensor based on micro-pyramid patterned ionic hydrogel for interactive human-machine interfaces. *Adv Sci* 2022;9:2104168. [DOI](#) [PubMed](#) [PMC](#)
43. Chhetry A, Kim J, Yoon H, Park JY. Ultrasensitive interfacial capacitive pressure sensor based on a randomly distributed microstructured iontronic film for wearable applications. *ACS Appl Mater Interfaces* 2019;11:3438-49. [DOI](#)
44. Luo G, Xie J, Liu J, et al. Highly conductive, stretchable, durable, breathable electrodes based on electrospun polyurethane mats superficially decorated with carbon nanotubes for multifunctional wearable electronics. *J Chem Eng* 2023;451:138549. [DOI](#)
45. Kim J, Zhang G, Shi M, Suo Z. Fracture, fatigue, and friction of polymers in which entanglements greatly outnumber cross-links. *Science* 2021;374:212-6. [DOI](#) [PubMed](#)
46. Brown AEX, Litvinov RI, Discher DE, Purohit PK, Weisel JW. Multiscale mechanics of fibrin polymer: gel stretching with protein unfolding and loss of water. *Science* 2009;325:741-4. [DOI](#) [PubMed](#) [PMC](#)
47. Wang X, Zhan S, Lu Z, et al. Healable, recyclable, and mechanically tough polyurethane elastomers with exceptional damage tolerance. *Adv Mater* 2020;32:2005759. [DOI](#)
48. Jeong JW, Yeo WH, Akhtar A, et al. Materials and optimized designs for human-machine interfaces via epidermal electronics. *Adv Mater* 2013;25:6839-46. [DOI](#)
49. Gu XW, Wu Z, Zhang YW, Srolovitz DJ and Greer JR. Microstructure versus flaw: mechanisms of failure and strength in nanostructures. *Nano Lett* 2013;13:5703-9. [DOI](#) [PubMed](#)
50. Ruth SRA, Bao Z. Designing tunable capacitive pressure sensors based on material properties and microstructure geometry. *ACS Appl Mater Interfaces* 2020;12:58301-16. [DOI](#) [PubMed](#)
51. Park J, Lee Y, Hong J, et al. Tactile-direction-sensitive and stretchable electronic skins based on human-skin-inspired interlocked microstructures. *ACS Nano* 2014;8:12020-9. [DOI](#)
52. Wu YG, Wang ZB, Xu JB, et al. Direct writing of liquid metal onto an electrospun graphene oxide composite polymer nanofiber membrane for robust and stretchable electrodes. *Adv Mater Technol* 2023;8:2201935. [DOI](#)